Journal of Power Sources 243 (2013) 913–918

Contents lists available at SciVerse ScienceDirect

Journal of Power Sources

journal homepage: www.elsevier.com/locate/jpowsour

Creep analysis of solid oxide fuel cell with bonded compliant seal design

Wenchun Jiang [a,*], Yucai Zhang [b], Yun Luo [a], J.M. Gong [c], S.T. Tu [b]

[a] State Key Laboratory of Heavy Oil Processing, College of Chemical Engineering, China University of Petroleum (East China), Qingdao 266555, PR China
[b] Key Laboratory of Pressure System and Safety (MOE), School of Mechanical and Power Engineering, East China University of Science and Technology, Shanghai 200237, PR China
[c] School of Mechanical and Power Engineering, Nanjing University of Technology, Nanjing 210009, PR China

HIGHLIGHTS

- Thermal stress induced creep in the SOFC with the BCS design is calculated.
- BCS design can decrease the thermal deformation by using creep effect.
- The failures would initiate at the middle of the cell edge and BNi-2.

ARTICLE INFO

Article history:
Received 31 January 2013
Received in revised form
13 June 2013
Accepted 13 June 2013
Available online 25 June 2013

Keywords:
Planar solid oxide fuel cell
Bonded compliant seal
Creep
Thermal stress

ABSTRACT

Solid oxide fuel cell (SOFC) requires good sealant because it works in harsh conditions (high temperature, thermal cycle, oxidative and reducing gas environments). Bonded compliant seal (BCS) is a new sealing method for planar SOFC. It uses a thin foil metal to bond the window frame and cell, achieving the seal between window frame and cell. At high temperature, a comprehensive evaluation of its creep strength is essential for the adoption of BCS design. In order to characterize the creep behavior, the creep induced by thermal stresses in SOFC with BCS design is simulated by finite element method. The results show that the foil is compressed and large thermal stresses are generated. The initial peak thermal stress is located in the thin foil because the foil acts as a spring stores the thermal stresses by elastic and plastic deformation in itself. Serving at high temperature, initial thermal displacement is partially recovered because of the creep relaxation, which becomes a new discovered advantage for BCS design. It predicts that the failures are likely to happen in the middle of the cell edge and BNi-2 filler metal, because the maximum residual displacement and creep strain are located.

1. Introduction

Planar solid oxide fuel cell (SOFC) is a clean energy conversion device which converts chemical energy into electrical energy directly by an electrochemical reaction [1]. But SOFC has not achieved large-scale commercialization because of its reliability and durability problems [2]. An important issue is the sealing technology due to operating at a harsh environment and high temperature [3]. It needs a good hermetic sealant to prevent the leakage of air and fuel, and effectively isolate the fuel from the oxidant.

There are two main types of seal: rigid seal and compressive seal [4]. For the rigid seal [5,6], metal, glass or glass–ceramic can be used to bond the components. But they are brittle and cracks will be generated after some thermal cycles. Silver or gold can be used for metal braze but they are too expensive. Now the researchers are trying to develop innovative self-healing glasses which can effectively heal the cracks during thermal cycling [1,7,8]. In recent years, F. Smeacetto et al. [9–14] have made great progress in life extension by designing several new composite sealants to produce a hermetic joint between the ceramic and metallic components. For the compressive seal [15–17], a compressive load is applied on SOFC stack to keep the tightness by using metals or mica-based composites as sealants. It doesn't bond the SOFC components rigidly together, but the applied load can be relaxed by creep, leading to the generation of leakage. In order to solve these problems, a third method named bonded compliant seal (BCS) has been developed

* Corresponding author. Tel./fax: +86 532 86983482.
E-mail addresses: jiangwenchun@upc.edu.cn, jiangwenchun@126.com (W. Jiang).

0378-7753/$ – see front matter Crown Copyright © 2013 Published by Elsevier B.V. All rights reserved.
http://dx.doi.org/10.1016/j.jpowsour.2013.06.096

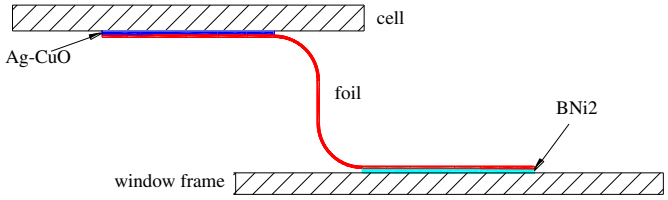

Fig. 1. The cross section of the BCS structure in planar SOFC.

by Weil et al. [18], which combines the advantages of both rigid and compressive seals. If the BCS method is proven to meet the stringent long-term operating requirements, it can be a good solution to the seal problem for SOFC applications.

In order to realize the use of BCS method, it is necessary to evaluate its mechanical performance and structure integrity [19–22], such as thermal stresses, residual stresses, creep and fatigue, etc. Weil et al. [23,24] performed a comparative finite element analysis of the stress–strain states in three different seal designs for SOFC, and found that the BCS design can accommodate a significant degree of thermal mismatch strain between the metallic support structure and the ceramic cell, and the thermal stresses in BCS design are much lower than those in glass–ceramic and brazed designs. Jiang and Chen [25] performed thermal stress analysis for an operating planar SOFC with BCS design by a thermo-electrochemical-structure model, and found that the thermal stress in the cell is relatively lower with a lower voltage, while the contribution of the temperature gradient to the thermal stress is higher. Jiang et al. [26] found that the Al_2O_3 protective film can generate a compressive stress on the surface of the foil. Jiang et al. [27,28] also investigated the as-bonded residual stress in planar SOFC with BCS design, and the effects of window frame material type, sealing foil thickness, filler metal thickness and window frame thickness on residual stresses have been discussed. The components of BCS design have different coefficients of thermal expansion (CTE), resulting in thermal stresses. The generated thermal stresses will induce creep deformation at high temperature [29]. Chiu and Lin [30] studied the thermo-mechanical fatigue properties of a ferritic stainless steel interconnect, and found that creep and creep–fatigue interaction are the two primary contributors to the fatigue damage. Therefore, a comprehensive analysis of creep behavior is necessary for evaluating the structural integrity of a planar SOFC with BCS design. In recent years, the creep study on SOFC are mainly focused on the interconnect [31], electrolyte [32], glass–ceramic seal materials [33], but little attention has been paid on BCS design. In this paper, creep analysis has been carried out to a planar SOFC with BCS design, which can provide a reference for the creep design.

2. Finite element creep analysis

2.1. Finite element model

Fig. 1 shows a cross section of the BCS structure in a planar SOFC. An S-shaped sealing foil is bonded to the cell and window frame by silver-based filler metal (Ag–4%CuO) and BNi-2 filler metal, respectively, which achieves the seal between cell and window frame. The materials of the foil and window frame are FeCrAlY and Haynes214, respectively. Their chemical compositions are listed in Tables 1–3, and mechanical strength is listed in Table 4.

At high temperature, thermal stresses will be generated because of the mismatching of CTE and subsequently induce creep

Table 1
Chemical composition of FeCrAlY (in wt%).

Fe	Cr	Al	Y	Mn	C	Si
≥69.62%	22%	4.8%	0.3%	≤0.04%	≤0.08%	≤0.70%

Table 2
Chemical composition of Haynes214 (in wt%).

Fe	Ni	Cr	Mo	Si	Mn	C	Co	B	P	Y	Zr
3	75	16	0.5	≤0.2	≤0.5	0.05	2	≤0.001	0.01	0.01	≤0.1

Table 3
Chemical composition of BNi-2 (in wt%).

C	Si	Mn	S	P	Cr	B	Ni	Fe	Mo
0.06	4.50	–	–	–	7.00	3.10	82.34	3.00	–

Table 4
Yield strength (20 °C) [23].

Material	FeCrAlY	Ag–4%CuO	BNi-2	Haynes214
Yield strength (MPa)	300	340	300	600

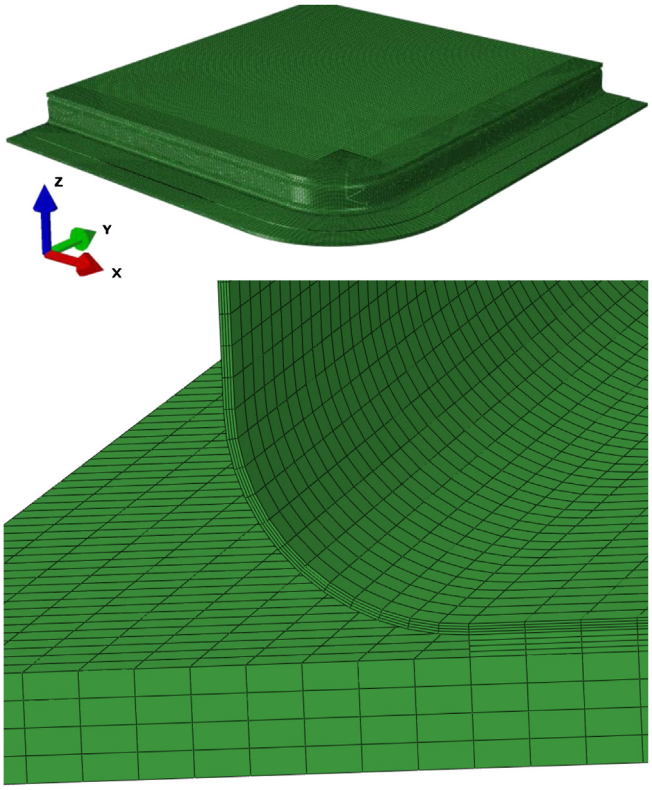

Fig. 2. Finite element meshing.

Table 5
Creep parameters (600 °C) [31,35–38].

Material	B (MPa^{-n} s^{-1})	n
FeCrAlY	2.251×10^{-29}	5.5
Haynes214	7.948×10^{-26}	6.896
BNi-2	2.431×10^{-43}	14.75
Ag–4%CuO	1.955×10^{-11}	1.867
Cell	2.64×10^{-11}	1.7

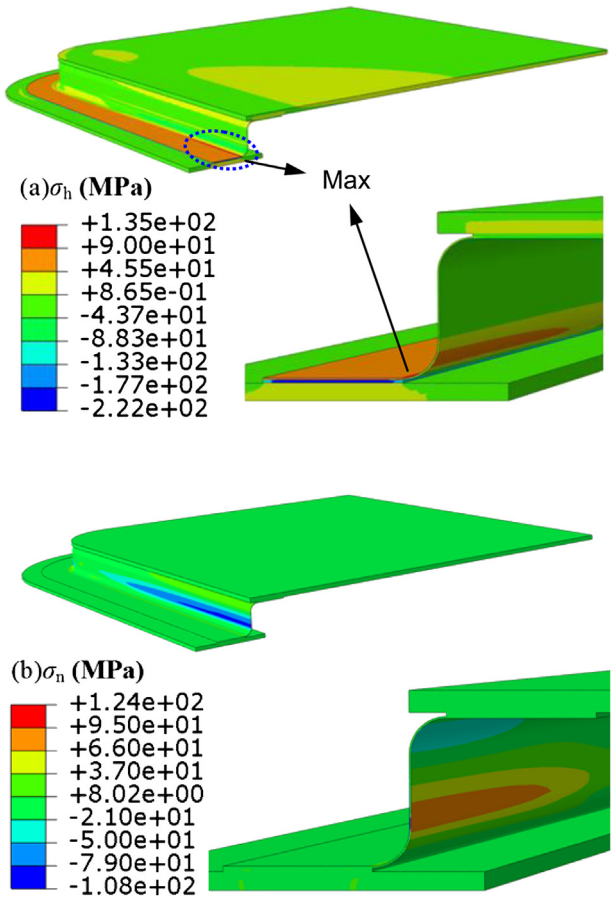

Fig. 3. Initial contour of hoop stress σ_h (a) and normal stress σ_n (b).

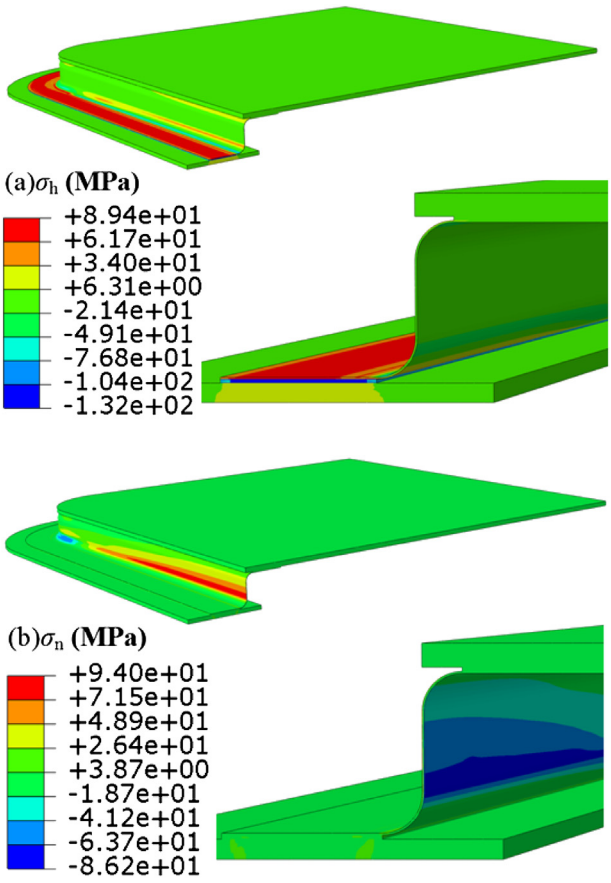

Fig. 5. Creep hoop stress σ_h (a) and normal stress σ_n (b) for a service of 50 000 h.

deformation, which is calculated by finite element code ABAQUS. A three dimensional finite element model is built and its meshing is shown in Fig. 2. In total, 249 047 nodes and 206 912 elements are meshed. The element type for thermal stress and creep calculation is C3D8. During the calculation, all the nodes on the bottom surface of the window frame were constrained in *Z*-direction, and the symmetric boundary conditions were applied on the two cross sections. Thus the rigid body motion was avoided. The first step is to calculate the thermal stress at 600 °C, and then the creep analysis of 50 000 h is carried out in the following step.

2.2. Thermal stress calculation

The thermal stresses affected by thermal-elasto-plasticity are simulated at an operating temperature of 600 °C. The elastic strain is modeled using the isotropic Hooke's law with temperature-dependent Young's modulus and Poisson's ratio. The thermal strain is calculated using the temperature-dependent CTE. For the plastic strain, a rate-independent plastic model is employed with Von Mises yield surface, temperature-dependent mechanical properties and isotropic hardening model. The required material properties are from Ref. [28].

2.3. Creep analysis

Creep is the time-dependent plastic strain at constant stress and temperature. The typical creep contains three phases: primary stage, secondary stage and tertiary stage. In the creep design, the primary and secondary stages are mainly considered. A commonly used equation of state representation of the two creep stages is described by Bailey–Norton law (power law creep law) [34].

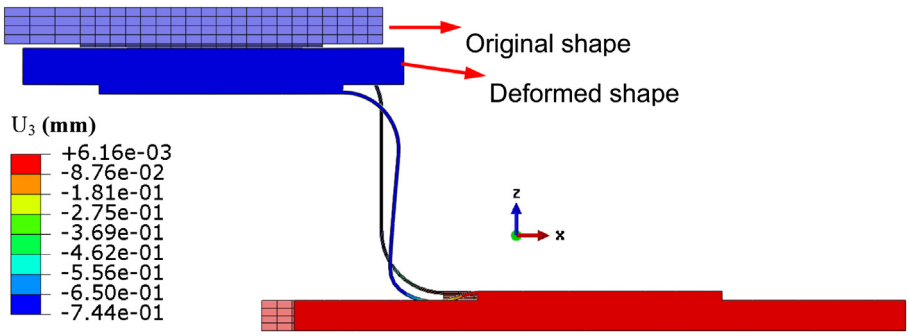

Fig. 4. Initial thermal displacement.

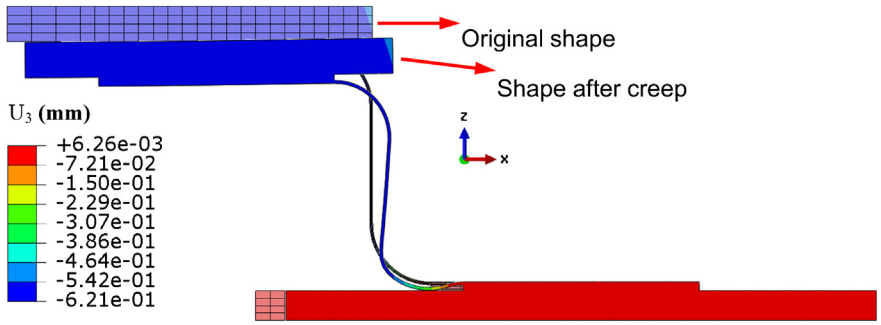

Fig. 6. Displacement after creep.

$$\dot{\varepsilon}_c = B\sigma^n \quad (1)$$

where the ε_c is the creep strain rate (s^{-1}); σ is stress (MPa); B and n are material constants listed in Table 5 [31,35–38]. The finite element creep analysis for 50 000 h is calculated at 600 °C.

3. Results and discussion

Here we define the stress along the circumferential of foil as the hoop stress (σ_h), and the stress along Z-direction (perpendicular to the cell) is defined as normal stress (σ_n). Because the stress along X-direction is similar to hoop stress. Therefore, only σ_h and σ_n are presented in the following discussion. Similarly, the creep strains along hoop and Z-directions are defined as hoop strain (ε_{ch}) and normal strain (ε_{cn}), respectively.

3.1. Initial thermal stress and deformation

The contour of initial hoop stresses (Fig. 3a) reveals that the mismatching of the mechanical properties generates large thermal stresses in the BCS structure. It is clearly shown that the stress distribution in the foil is not uniform, with a maximum value of 135 MPa being reached at the connection between the lower horizontal part and the quarter-circle of the foil. In the horizontal part of the foil connected to the filler metal BNi-2, the hoop stress is tensile (~80 MPa). In the vertical part of the foil, the hoop stress in the out surface is compressive while it is tensile in the lower part of the inner surface. BNi-2 has a compressive stress (~−222 MPa), because it has a bigger CTE than the neighboring metals and is constrained by the adjacent metals. The hoop stresses are about 20, −20 and 30 MPa in the cell, silver filler metal and window frame, respectively.

Fig. 3b shows the contour of normal hoop stresses. A tensile stress peak of ~124 MPa is shown at the inner surface of the vertical foil, while a compressive stress peak is formed in the outside surface of the vertical foil. The bottom surface of the window frame is constrained in Z-direction and the cell has a smaller CTE than the foil metal, which constrains the expansion of the foil. The thermal compressive stresses originated about 0.74 mm shrinkage at the cell edge along Z-direction as shown in Fig. 4. Along X-direction the BCS structure also underwent a bowing deformation that can relax some thermal stresses in X-direction as shown in Fig. 4. The normal stresses in other components are very small, proving the advantage

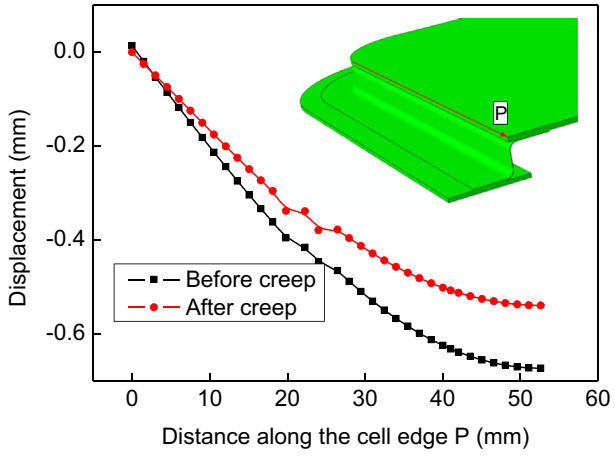

Fig. 7. Displacement along the cell edge.

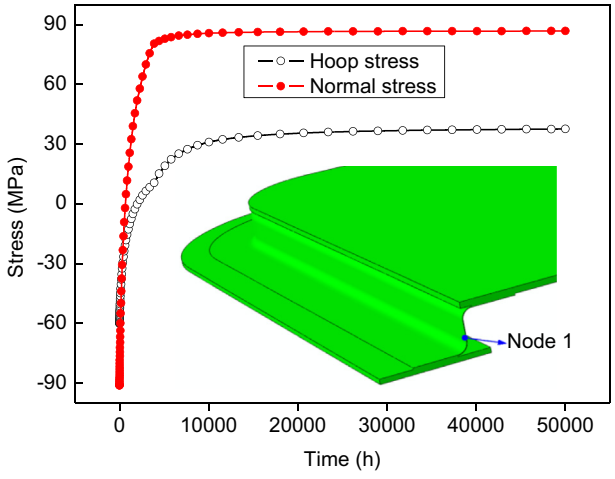

Fig. 9. The creep stress changing with time of node 1 in the foil.

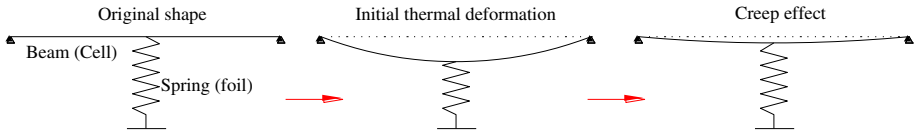

Fig. 8. A simplified stress model of the BCS design.

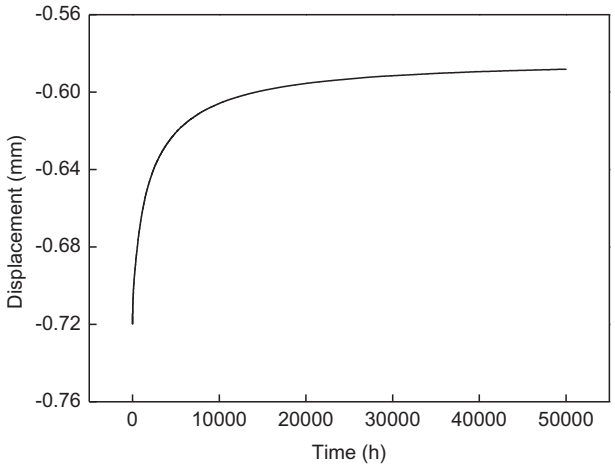

Fig. 10. The foil displacement changing with time.

of the BCS design. Acting as a spring, the foil can absorb the thermal stresses by elastic and plastic deformation.

3.2. Creep stress and deformation

Fig. 5 shows the hoop and normal creep stresses. Due to the effect of creep, the stresses are redistributed greatly. The hoop and normal peak stresses decrease to 89.4 and 94 MPa, respectively, and the initial compressive hoop stress in BNi-2 decreases to −132 MPa. The normal stresses in the vertical foil have changed completely, with tensile stress (∼94.1 MPa) in the outside surface and compressive stress in the inner surface (∼−86.2 MPa) as shown in Fig. 5b, which is completely different from the initial condition: compressive stress in the outside and tensile stress in the inner surface as shown in Fig. 3b.

After a service of 50 000 h as illustrated in Fig. 6, the compressive displacement at the cell edge is about 0.62 mm, which decreases about 16% compared to the initial thermal displacement (Fig. 4). Fig. 7 shows the displacement before and after creep along the cell edge (path P shown in Fig. 7), clearly proving that the displacement decreases greatly because of the creep effect. The cell is supported by the foil and has a high constraint at the ends, making this structure similar to a simply supported beam. Therefore, the maximum displacement is shown in the middle and then decreases gradually to the ends.

3.3. Discussion

From the above results, it shows that by using the creep effect, the BCS design can decrease the cell displacement. Fig. 8 shows a simplified stress model of the BCS design. The cell likes a simply supported beam, and the foil likes a spring. At the beginning, the foil has a compressive thermal displacement. But after operating for some time at high temperature, the stresses in the foil are relaxed, recovering part compressive displacement. Fig. 9 shows the creep stress changing with time for node 1 (marked in Fig. 9) in the vertical part of foil. It clearly shows that the compressive stress decreases to zero quickly and then changes to tensile stress over time. Finally, the hoop and normal stresses increase to ∼90 and 30 MPa, respectively. As the compressive stress is relaxed, the foil is elongated to decrease the compressive displacement gradually, verifying the foil creep can recover part of the cell displacement, as

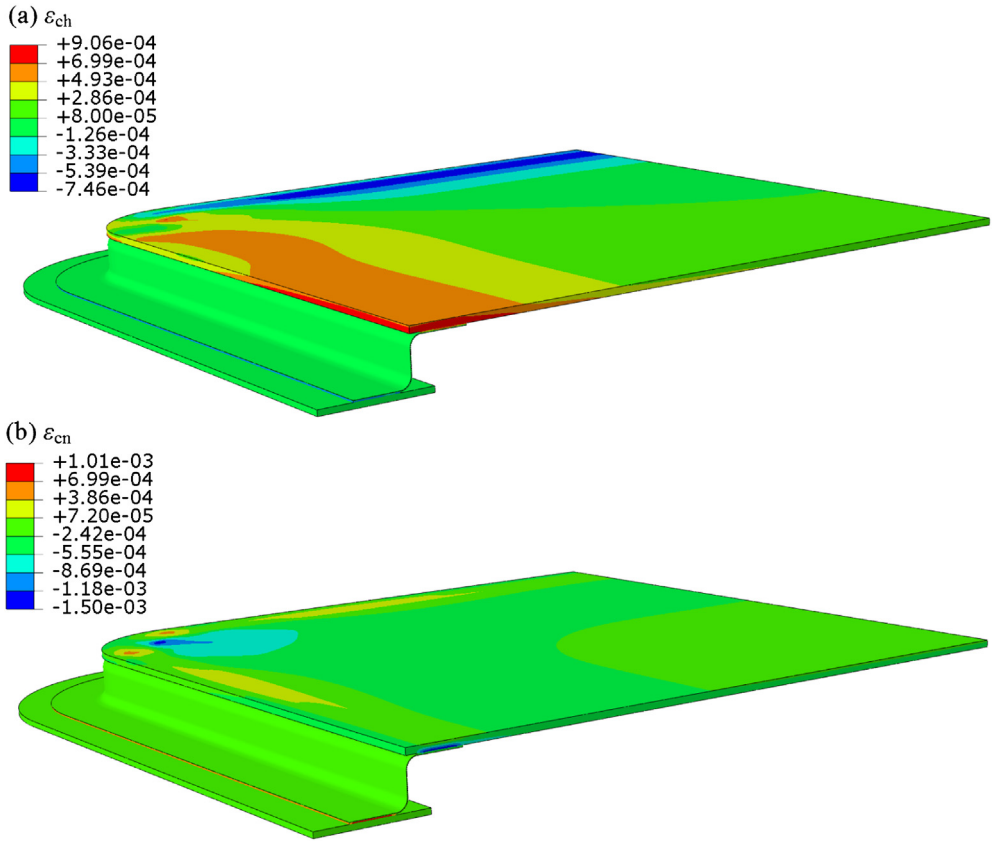

Fig. 11. Contour of hoop strain ε_{ch} (a) and normal strain ε_{cn} (b).

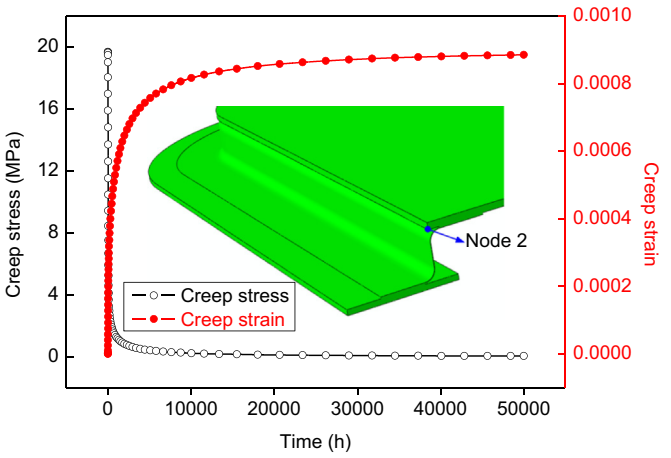

Fig. 12. Creep stress and strain changing with time of node 2 in the middle of cell edge.

shown in Fig. 10. This is a new discovered advantage for BCS structure. But the compressive displacement of the foil cannot recover completely because of the plastic deformation, and the residual displacement is about 0.6 mm, as shown in Fig. 10. That is to say, the cell deformation is mainly contributed by the thermal deformation.

Fig. 11 shows the creep contour, and Fig. 12 shows the creep stress and strain changing over time for node 2 (marked in Fig. 12) in the middle of cell edge. The peak hoop creep strain is located at the middle of the cell edge (Fig. 11a). In the cell, the stresses are relaxed and reach almost zero finally, resulting the increase of the creep strain, as shown in Fig. 12. In addition, the maximum residual displacement is also in the middle of cell edge, as shown in Fig. 7. Therefore, we can predict that the failure would be likely to happen in the middle of cell edge. BNi-2 filler metal also becomes a potential source of creep failure. Because the foil is elongated and generates a tension to BNi-2. As a result, the maximum tensile normal creep is located in BNi-2, as shown in Fig. 11b.

4. Conclusions

This study performs a creep analysis induced by thermal stresses to the planar SOFC with BCS design. Based on this study the following conclusions could be achieved.

(1) Due to the mismatching of mechanical properties, large thermal stresses and thermal displacement are generated in BCS design at high temperature. The maximum initial thermal displacement is located in the middle of cell edge, and the peak thermal stress is stored in the foil because the foil likes a spring which absorbs the thermal stress by elastic and plastic deformation in itself.
(2) At high temperature, the stress in the foil is relaxed by creep, and the initial compressive thermal displacement of the foil is partially recovered, which leads to a decrease of displacement in the cell. By using the creep effect, the BCS design can decrease 16% of the cell deformation, which is a new discovered advantage of the BCS design.
(3) Both the middle of the cell edge and BNi-2 are the potential failure positions, because the maximum residual deformation and hoop creep strain are found at the middle of the cell edge, and the maximum normal creep strain is in the BNi-2.

Acknowledgments

The authors gratefully acknowledge the support provided by the National Natural Science Foundation of China (51105380), Doctoral Program of Higher Education of China (20100133120008), Natural Science Foundation of Shandong Province (ZR2010AQ002), Fundamental Research Funds for the Central Universities (12CX02006A) and Key Laboratory of Pressure System and Safety (MOE), East China University of Science and Technology.

References

[1] Wei Xu, Xin Sun, Elizabeth Stephens, Loannis Mastorakos, Mohammad A. Khaleel, Hussein Zbib, J. Power Sources 218 (2012) 445–454.
[2] Arata Nakajo, Fabian Mueller, Jacob Brouwer, Jan Van Herle, Daniel Favrat, J. Power Sources 216 (2012) 449–463.
[3] Chih Kuang Lin, Ling Hao Huang, Lieh Kwang Chiang, Yau Pin Chyou, J. Power Sources 192 (2) (2009) 515–524.
[4] M.K. Mahapatra, K. Lu, J. Power Sources 195 (21) (2010) 7129–7139.
[5] Jean Duquette, Anthony Petric, J. Power Sources 137 (1) (2004) 71–75.
[6] Shaobai Sang, Jian Pu, Chi Bo, Li Jian, J. Power Sources 193 (2) (2009) 723–729.
[7] Teng Zhang, Qi Zou, Jing Zhang, Dian Tang, Hiswen Yang, J. Power Sources 204 (2012) 122–126.
[8] W.N. Liu, X. Sun, M.A. Khaleel, J. Power Sources 196 (4) (2011) 1750–1761.
[9] F. Smeacetto, M. Salvo, F.D. D'Hérin Bytner, P. Leone, M. Ferraris, J. Eur. Ceram. Soc. 30 (4) (2010) 933–940.
[10] F. Smeacetto, A. Chrysanthou, M. Salvo, Z. Zhang, M. Ferraris, J. Power Sources 190 (2) (2009) 402–407.
[11] F. Smeacetto, M. Salvo, M. Santarelli, P. Leone, G.A. Ortigoza-Villalba, A. Lanzini, L.C. Ajitdoss, M. Ferraris, Int. J. Hydrogen Energy 38 (1) (2013) 588–596.
[12] F. Smeacetto, M. Salvo, M. Ferraris, V. Casalegno, P. Asinari, J. Eur. Ceram. Soc. 28 (3) (2008) 611–616.
[13] F. Smeacetto, A. Chrysanthou, M. Salvo, T. Moskalewicz, F. D'Herin Bytner, L.C. Ajitdoss, M. Ferraris, Int. J. Hydrogen Energy 36 (18) (2011) 11895–11903.
[14] F. Smeacetto, M. Salvo, P. Leone, M. Santarelli, M. Ferraris, Mater. Lett. 65 (6) (2011) 1048–1052.
[15] Shiru Le, Kening Sun, Naiqing Zhang, Yanbin Shao, Maozhong An, Qiang Fu, Xiaodong Zhu, J. Power Sources 168 (2) (2007) 447–452.
[16] Zhou Dai, Jian Pu, Dong Yan, Bo Chi, Li Jian, Int. J. Hydrogen Energy 36 (4) (2011) 3131–3137.
[17] Yeong Shyung Chou, Jeffry W. Stevenson, J. Power Sources 115 (2) (2003) 274–278.
[18] K. Scott Weil, John S. Hardy, Brian J. Koeppel, J. Mater. Eng. Perform. 15 (4) (2006) 427–432.
[19] Arata Nakajo, Jakob Kuebler, Antonin Faes, Ulrich F. Vogt, Hans Jürgen Schindler, Lieh-Kwang Chiang, Stefano Modena, Jan Van Herle, Thomas Hocker, Ceram. Int. 38 (5) (2012) 3907–3927.
[20] Arata Nakajo, Zacharie Wuillemin, Jan Van Herle, Daniel Favrat, J. Power Sources 193 (1) (2009) 203–215.
[21] Chih Kuang Lin, Jun Yu Chen, Jie Wun Tian, Lieh Kwang Chiang, Si Han Wu, J. Power Sources 205 (2012) 307–317.
[22] Arata Nakajo, Fabian Mueller, Jacob Brouwer, Jan Van Herle, Daniel Favrat, J. Power Sources 216 (2012) 434–448.
[23] K.S. Weil, B.J. Koeppel, J. Power Sources 180 (1) (2008) 343–353.
[24] K.S. Weil, B.J. Koeppel, Int. J. Hydrogen Energy 33 (14) (2008) 3976–3990.
[25] Tsung Leo Jiang, Ming Hong Chen, Int. J. Hydrogen Energy 34 (19) (2009) 8223–8234.
[26] Wenchun Jiang, Yucai Zhang, Wanchuck Woo, S.T. Tu, J. Power Sources 196 (24) (2011) 10616–10624.
[27] Wenchun Jiang, S.T. Tu, G.C. Li, J.M. Gong, J. Power Sources 195 (11) (2010) 3513–3522.
[28] Wenchun Jiang, Yucai Zhang, Wanchuck Woo, S.T. Tu, J. Power Sources 209 (2012) 65–71.
[29] Yung Tang Chiu, Chih-Kuang Lin, J. Power Sources 198 (2012) 149–157.
[30] Yung-Tang Chiu, Chih-Kuang Lin, J. Power Sources 219 (2012) 112–119.
[31] Yung Tang Chiu, Chih Kuang Lin, Jiunn Chi Wu, J. Power Sources 196 (4) (2011) 2005–2012.
[32] J. Laurencin, G. Delette, F. Usseglio-Viretta, S. Di Iorio, J. Eur. Ceram. Soc. 31 (9) (2011) 1741–1752.
[33] Jacqueline Milhans, Mohammed Khaleel, Xin Sun, Mehran Tehrani, Marwan Al-Haik, H. Garmestani, J. Power Sources 195 (11) (2010) 3631–3635.
[34] Farid Vakili Tahami, Amir Hossein Daei-Sorkhabi, Farid Reza Biglari, Mater. Sci. Eng. A 527 (18–19) (2010) 4993–4999.
[35] S.J. Bull, Oxid. Met. 49 (1998) 1–17.
[36] Wenchun Jiang, Jianming Gong, Hu Chen, S.T. Tu, Int. J. Pressure Vessels Piping 85 (8) (2008) 569–574.
[37] Mansur Akbari, Sebastian Buhl, Christian Leinenbach, Ralph Spolenak, Konrad Wegener, Mech. Mat. 52 (1) (2012) 69–77.
[38] Yu Jinjiang, Sun Xiaofeng, Jin Tao, Zhao Nairen, Guan Hengrong, Hu Zhuangqi, Mat. Sci. Eng. A 527 (9) (2010) 2379–2389.